BMC Veterinary Research

RESEARCH

Open Access

TMT-based quantitative proteomics reveals the targets of andrographolide on LPS-induced liver injury

Shihao Ge[1,2], Wenqi Lian[1], Yongjiang Bai[1], Linzheng Wang[3], Fuwei Zhao[2], Houmei Li[4], Dongliang Wang[5] and Quanhai Pang[1*]

Abstract

Background Andrographolide (Andro) is a diterpenoid derived from Andrographis paniculate, which has anti-inflammatory, antibacterial, antiviral and hepatoprotective activities. Gram-negative bacterial infections can cause varying degrees of liver injury in chickens, although Andro has been shown to have a protective effect on the liver, its underlying mechanism of action and effects on liver proteins are not known.

Methods The toxicity of Andro on the viability of leghorn male hepatoma (LMH) cells at different concentrations and times was analyzed by CCK-8 assays. Alanine aminotransferase (ALT) and aspartate aminotransferase (AST) activities in the culture supernatants were measured using an automatic biochemical analyzer to evaluate the protective effect of androscopolide on LPS-induced injury of LMH cells. Subsequently, TMT proteomics analysis were performed on the negative control group (NC group), LPS, and LPS-Andro groups, and bioinformatics analysis was performed on the differentially expressed proteins (DEPs).

Results It was found that Andro reduced ALT and AST levels in the cell supernatant and alleviated LPS-induced injury in LMH cells. Proteomic analysis identified 50 and 166 differentially expressed proteins in the LPS vs. NC group and LPS-Andro vs. LPS group, respectively. Andro may be involved in steroid metabolic processes, negative regulation of MAPK cascade, oxidative stress, and other processes to protect against LPS-induced liver injury.

Conclusions Andro protects against LPS-induced liver injury, HMGCS1, HMGCR, FDPS, PBK, CAV1, PRDX1, PRDX4, and PRDX6, which were identified by differential proteomics, may be the targets of Andro. Our study may provide new theoretical support for Andro protection against liver injury.

Keywords Proteomics, Andrographolide, LPS, Liver injury, Targets

*Correspondence:
Quanhai Pang
pangquanhai@163.com
[1]College of Veterinary Medicine, Shanxi Agricultural University, Taigu 030801, Shanxi, China
[2]College of Pharmacy, Heze University, Heze 274000, Shangdong, China
[3]College of Traditional Chinese Medicine, Shandong University of Traditional Chinese Medicine, Jinan 250035, Shangdong, China
[4]Shuozhou grass and animal husbandry development center, ShuoZhou 036000, Shanxi, China
[5]ShuoZhou Vocational Technology College, ShuoZhou 036000, Shanxi, China

Background

The liver is essential for biotransformation and toxin removal [1]. Gram-negative bacteria are common pathogens that infect chickens, leading to decreased productivity and even death of the chickens, with severe losses to the chicken industry. Studies have found that many Gram-negative bacteria can cause varying degrees of liver injury in chickens [2–4]. Lipopolysaccharide (LPS) forms part of the cell walls of Gram-negative bacteria, where it interacts with the host during the infection process [5]. Pathogen pattern recognition receptors (PRRs) on the host cell surfaces recognize LPS, triggering an innate immune response by activating signaling pathways and stimulating pro-inflammatory cytokine production to defend against the bacterial invasion [6]. Toll-like receptors (TLRs) are a type of PRR and TLR4 is especially involved in the response to LPS. TLR4 recognizes LPS to activate mitogen-activated protein kinase (MAPK), leading to an up-regulation of inflammatory mediators, including tumor necrosis factor-α (TNF-α), and potentially causing inflammatory liver injury [7]. Furthermore, LPS can stimulate the production of reactive oxygen species (ROS) which, if not removed by the antioxidant defense system can lead to oxidative stress [8]. Studies have found that inflammation is usually accompanied by the formation of ROS and oxidative stress [9], and both are closely involved in inflammatory liver injury. Therefore, oxidative stress is considered to mediate the development of liver injury [10].

Traditional Chinese medicine (TCM) targets multiple pathways and proteins in the treatment of disease, using complex and diverse mechanisms of action. Proteomics provides a powerful means of studying the possible mechanisms of TCM, and many researchers have studied the potential targets of TCM in different diseases using proteomics technology [11–13]. Thus, proteomics is helpful to identify the potential target proteins or biomarkers associated with TCM treatment. Andrographolide (Andro) is a diterpenoid derived from *Andrographis paniculate* and is documented to have a variety of physiological effects, including anti-inflammatory, antiviral, antitumor, and immune regulatory properties [14]. Andro is also effective for hepatoprotection [15] and reduces the levels of alanine aminotransferase (ALT), aspartate aminotransferase (AST), interleukin (IL)-1β, and TNF-α in liver tissue by inhibiting nuclear factor-Kappa B (NF-κB) and activating the nuclear factor erythroid 2-related factor 2 (Nrf2) signaling pathway, thus protecting against liver damage resulting from by D-GalN/LPS treatment in mice [16]. Andro can also protect against cholestatic liver damage by reducing oxidative stress and inflammation [17]. However, Andro-mediated protection against LPS-induced liver damage has not been investigated using proteomics.

In this study, based on tandem mass tag (TMT) proteomics, we investigated the effects of Andro on LPS-induced liver damage in immortalized chicken leghorn male hepatoma (LMH) cells. Differentially expressed proteins (DEPs) were identified and further analyzed by Gene Ontology (GO) and Kyoto Encyclopedia of Genes and Genomes (KEGG) to gain insight into potential targets of Andro for protection against LPS-induced liver damage.

Results

Toxicity of Andro on the viability of LMH cells

CCK-8 assays confirmed that the concentrations of Andro used for experiments did not reduce the viability of the cells. As shown in Fig. 1, the Andro concentrations used were 0, 1, 5, 10, 20, 50, 100, 200, and 400 μM, with times of 0, 12, 24, 48, 72, and 96 h. Andro was found to lower the viability of LMH cells in a time- and dose-dependent manner, with no significant differences seen between the different Andro concentrations at 0 h ($P>0.05$). 12, or 24 h, Andro was found to be cytotoxic at concentrations greater than 10 μM. Therefore, concentrations of 1–5 μM which showed less cytotoxicity were selected for the following experiments.

Influence of Andro on ALT and AST in LMH culture supernatants after LPS challenge

ALT and AST activities are frequently used to indicate liver injury in clinical practice. Significant increases in both ALT and AST were observed after 24-h LPS challenge in LMH cells ($P<0.001$), with different concentrations of Andro (1, 2, and 5 μM) leading to gradual reductions in ALT and AST activities and reaching significance ($P<0.001$) at 5 μM Andro (Fig. 2). Therefore, 24 h, 5 μM Andro was used for proteomic assays.

Differences in protein expression induced by LPS and andro

DEPs were screened between the LPS vs. NC groups and the LPS-Andro vs. LPS groups, using the thresholds of $P<0.05$ and Fold Change (FC) >1.2 or $<1/1.2$. As shown in Fig. 3A-C, LPS significantly altered the protein levels in the LMH cells, compared with the NC group. Altogether, 50 DEPs were identified in the LPS group, of which 27 were up-regulated and 23 were down-regulated. Andro treatment significantly changed the numbers of DEPs, with 166 DEPs identified in comparison with the LPS group, of which 77 were up-regulated and 89 were down-regulated. The detailed information of DEPs is listed in Supplementary Table 1.

Subcellular localization of the DEPs

The subcellular localizations, as well as the numbers of up-and down-regulated proteins, were analyzed using

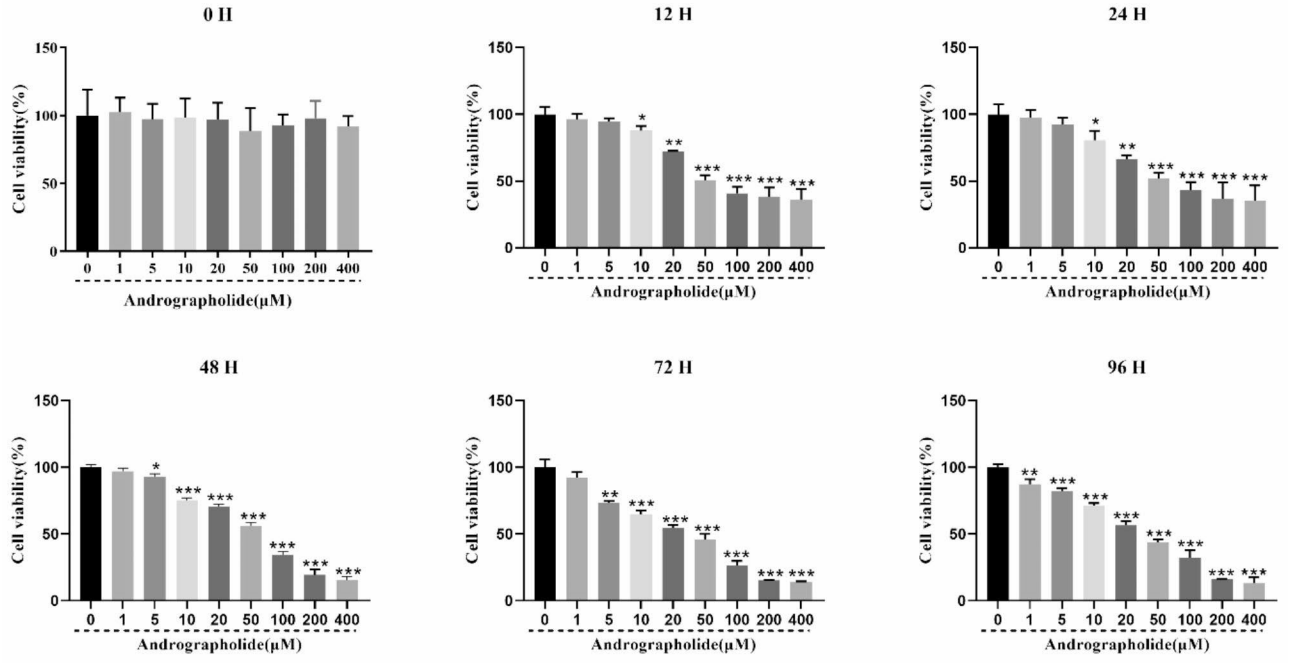

Fig. 1 The cell viability of Andro on LMH cells. LMH cells were treated with different concentrations of Andro (0, 1, 5, 10, 20, 50, 100, 200 and 400 μM) for different time points (0, 12, 24, 48, 72 and 96 h), cell viability was measured using the CCK8 assay. (* $P<0.05$, ** $P<0.01$, *** $P<0.001$ vs. 0 μM)

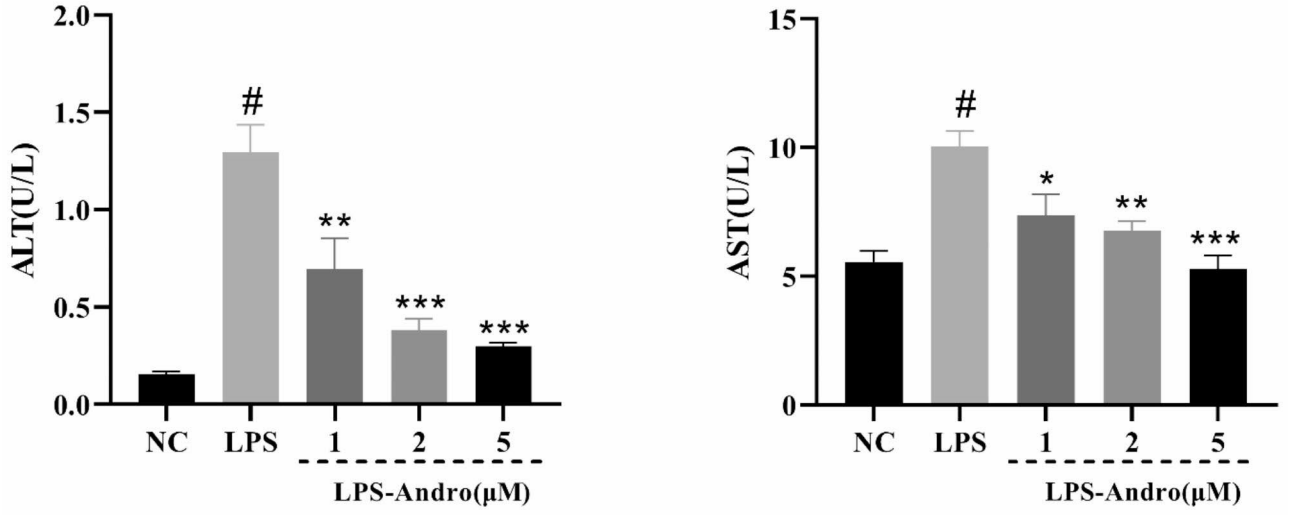

Fig. 2 Effects of Andro on LPS-induced LMH cells supernatant AST (**A**) and ALT (**B**) levels. # $P<0.001$ vs. NC, * $P<0.05$, ** $P<0.01$, *** $P<0.001$ vs. LPS

PSORTb and WoLF PSORT soft, respectively. Figure 4 A showed the subcellular localizations of 27 proteins that were up-regulated and 23 that were down-regulated after LPS treatment. Of the 27 up-regulated proteins, nine were nuclear, eight were cytoplasmic, four were extracellular, and four were mitochondrial. Of the 23 down-regulated proteins, nine were nuclear, five were cytoplasmic, three were extracellular, and two were mitochondrial. Of the proteins expressed differentially between the LPS-Andro and LPS groups, as shown in Fig. 4B, the 77 up-regulated proteins were expressed predominantly in the cytoplasm, with 39 proteins, followed by the nucleus with 18, the mitochondria with five, and the extracellular environment with four proteins. Of the 89 down-regulated proteins, 35 were nuclear, 26 were cytoplasmic, 12 were extracellular, and six were mitochondrial.

GO analysis of DEPs

The DEPs were classified into the biological process (BP), cellular component (CC), and molecular function (MF) categories according to their GO annotations. As illustrated in Fig. 5A, LPS-treated cells, compared with

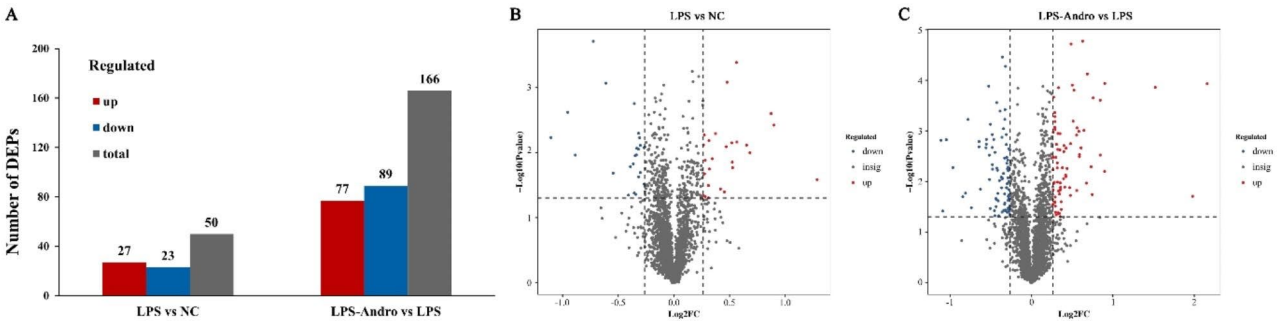

Fig. 3 The number of significant differentially expressed proteins in 3 group. (**A**) The number of significant differentially expressed proteins between in LPS vs. NC group and LPS-Andro vs. LPS group (Blue represents down-regulated proteins, red represents up-regulated proteins, and gray represents total proteins); (**B**) Volcano plot of proteins identified from LPS and NC group; (**C**) Volcano plot of proteins identified from LPS-Andro and LPS group. (The abscissa of the volcano plot represents log2 of the Fold Change, the ordinate represents -log10 *P* value, red and blue scatter points represent up-regulated and down-regulated proteins, respectively, and gray represents non-significantly expressed proteins)

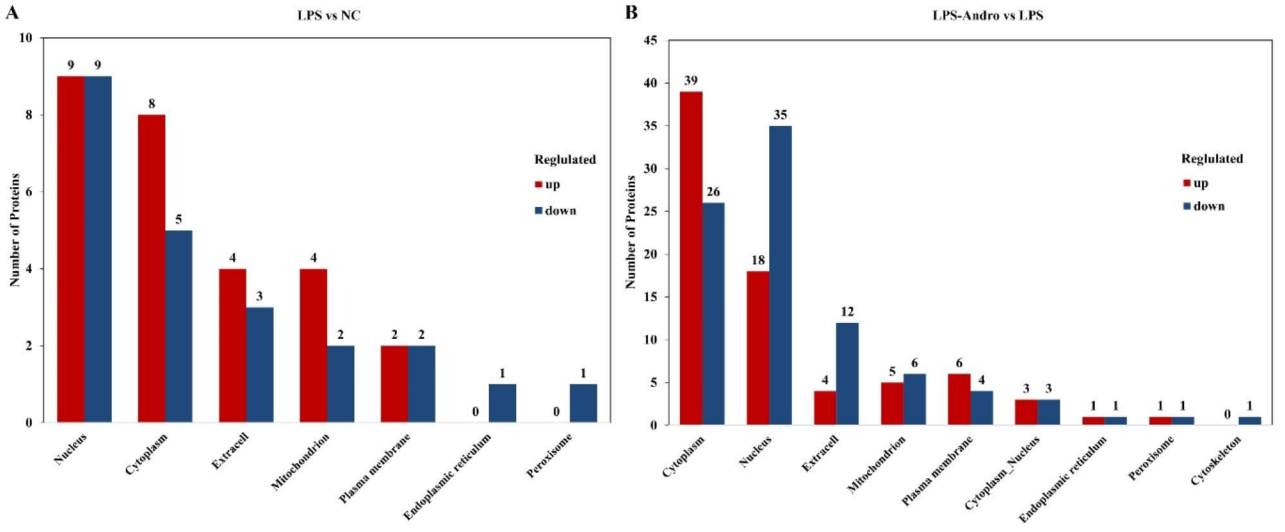

Fig. 4 Subcellular localization of differential proteins, the abscissa represents the subcellular fraction, the ordinate represents the number of differential proteins, and the red and blue represent up-regulated and down-regulated differential proteins, respectively. (**A**) LPS vs. NC; (**B**) LPS-Andro vs. LPS

the NC group, showed enrichment in the BP category, including processes such as signal transduction, immune response, responses to external stimuli, and inflammatory response. In the MF category, the DEPs between these two groups were mostly involved in signal receptor binding, lipid binding, and phospholipid binding. Figure 5B shows the comparison between the LPS and LPS-Andro groups; it can be seen that Andro induced the expression of proteins in the BP category related to phosphorus, carbohydrate, and steroid metabolism, as well as negative regulation of MAPK cascade, amongst others. In the MF category, the DEPs were mostly connected to oxidoreductase activity, receptor regulation, and antioxidant activity.

KEGG pathway analysis of the DEPs

Further exploration of the signaling pathways underlying the effects of LPS and Andro was conducted by KEGG analysis of enriched pathways. The 50 DEPs identified after LPS treatment, compared with NC cells, were associated with 92 KEGG pathways, including the Rap1, phosphatidylinositol 3-kinase (PI3K)-protein kinase B (AKT), NF-κB, and MAPK signaling pathways (Fig. 6A). Compared with the LPS group, the 166 DEPs identified in the LPS-Andro group were involved in 223 KEGG pathways, with those of interest including pathways associated with metabolism and hypoxia-inducible factor-1 (HIF-1) signaling (Fig. 6B).

PPI analysis of DEPs

Using the StringDB database, we constructed a PPI network for the identified DEPs. Our results showed that App, NFκB2, RELB, TRAF3, and FGF2 played vital roles in the network after LPS treatment, as shown in Fig. 7A. After Andro treatment, the major proteins were PRDX1,

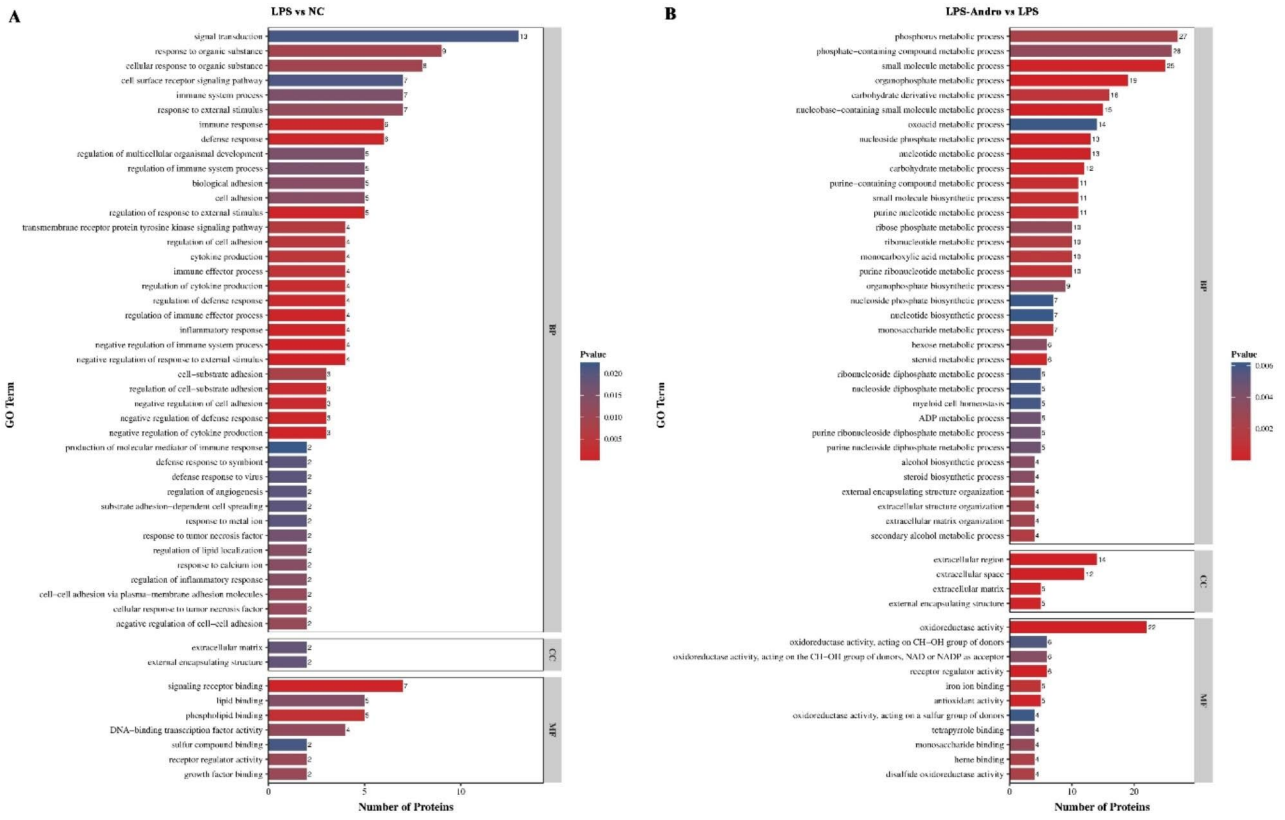

Fig. 5 GO enrichment results of the DEPs, the abscissa represents the number of differentially annotated proteins, the ordinate represents the enriched GO entries, and the color change from blue to red represents the change of P-value from large to small. (BP: biological process; CC: cell component; MF: molecular function). (**A**) LPS vs. NC; (**B**) LPS-Andro vs. LPS

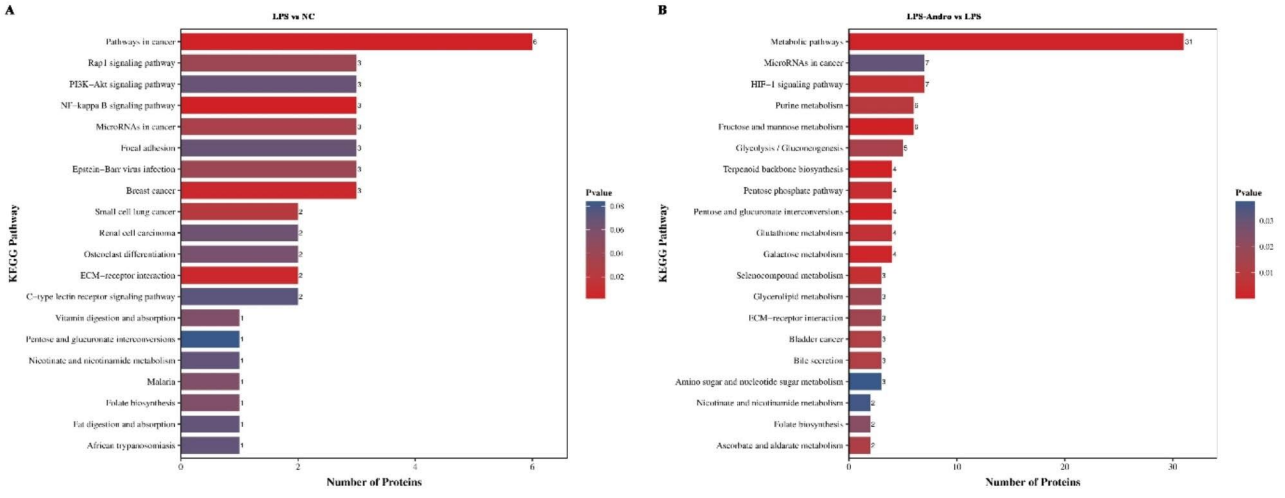

Fig. 6 KEGG enrichment results of the DEPs, the abscissa represents the number of differentially annotated proteins, the ordinate represents the enriched KEGG pathway, and the color change from blue to red represents the change of P-value from large to small. (**A**) LPS vs. NC; (**B**) LPS-Andro vs. LPS

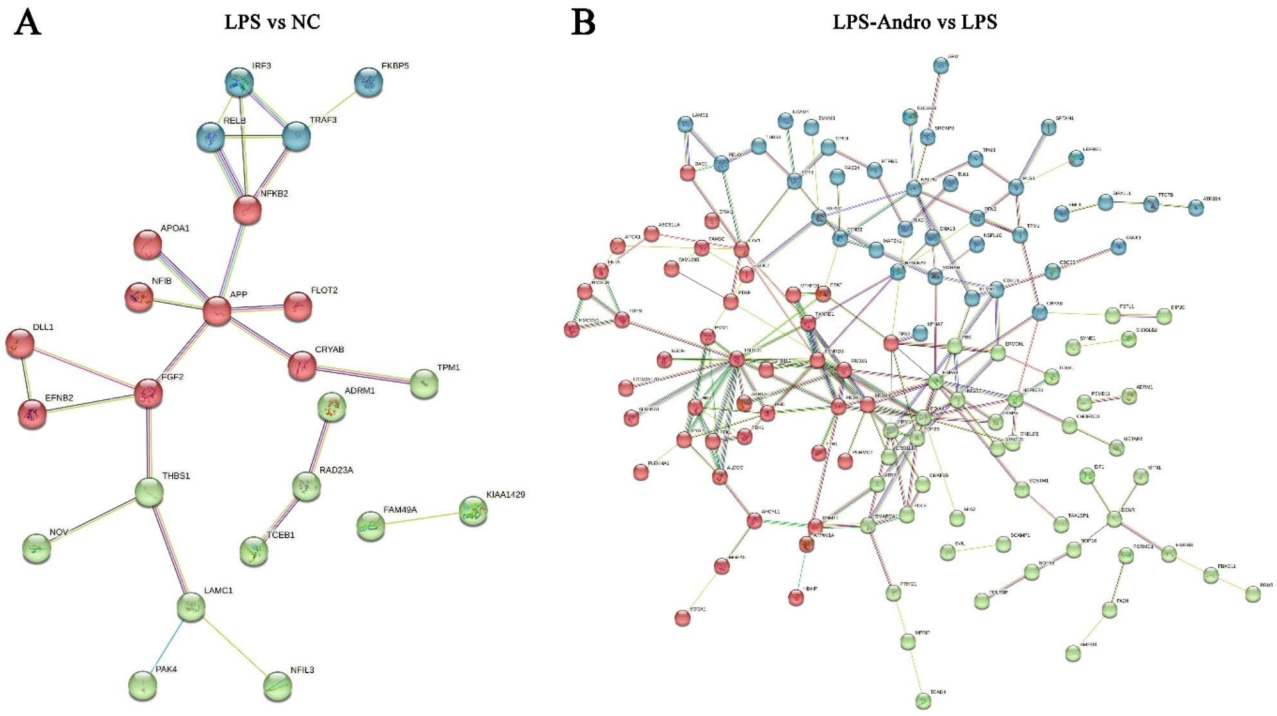

Fig. 7 Protein-protein interaction networks built on STRING for the identified proteins. (**A**) LPS vs. NC; (**B**) LPS-Andro vs. LPS, different colors represent the three clusters distinguished by the K-means method

PRDX4, PRDX6, PBK, and CAV1 (see Fig. 7B), which may be associated with oxidative stress and MAPK signaling.

Discussion

The innate immune system is the main defense against microorganisms, and LPS can act as an inducer of innate immunity to activate the adaptive immune system [18]. LPS binds to the PRR TLR4 to activate MAPK and NF-κB signaling [19, 20], as well as the PI3K-AKT pathway [21], generating an inflammatory response. Consistent with this, the KEGG analysis indicated that LPS activated Rap1, PI3K-Akt, NF-κB, and MAPK signaling in LMH cells. GO analysis of the 50 DEPs between the LPS and NC groups indicated that they tended to be involved in biological processes such as the immune and inflammatory responses and responses to external stimuli such as TRAF3 and RELB. Proteins belonging to the tumor necrosis factor receptor (TNF-R)-associated factor (TRAF) family function in a variety of signal transduction pathways leading to the expression of a variety of immune receptors, including innate and adaptive and cytokine receptors [22]. TRAF3 signaling stimulates the NF-κB and MAPK pathways, both of which regulate inflammation and the inflammatory response [23, 24]. RELB, a member of the NF-κB transcription factor family, is significantly up-regulated during inflammation, which induces the formation of the RELB/p50/IκBα complex [25]. It was found that LPS caused upregulation of TRAF3 in human bronchial epithelium (16HBE) [26] and also increased RELB expression in RAW 264.7 cells [27]; our results are in agreement with these findings.

The 166 DEPs identified after Andro treatment, compared with cells treated only with LPS, were found to be involved in 223 KEGG pathways, with significant enrichment seen in pathways associated with metabolism and HIF-1 signaling. GO analysis indicated DEP involvement in biological processes such as steroid and carbohydrate metabolism and the negative regulation of MAPK cascades. HIF is a heterodimeric complex composed of α and β subunits, with the α subunit having two forms, HIF-1α and HIF-2α. HIF-1α is a key regulator of both cell metabolism and inflammation [28, 29], and LPS can activate the expression of HIF-1α [30]. Studies have shown that there are close relationships between HIF-1α, inflammation, and cholesterol metabolism [31–34]. Cholesterol accumulation in macrophages can augment the inflammatory response [32], promoting HIF-1 activation, and may mediate liver injury [33]. Some TCM can inhibit inflammation by interfering with HIF-1α; for example, curcumin can reduce inflammation and apoptosis by inhibiting HIF-1α expression and the total cholesterol content in macrophages [35]. Our results showed that Andro down-regulated the expression of HMGCS1, HMGCR, and FDPS involved in steroid metabolism. The mevalonate pathway is involved in lipid metabolism and is a key regulatory step in the de novo synthesis of

cholesterol, with 3-hydroxy-3-methylglutaryl coenzyme A synthase 1(HMGCS1) and 3-hydroxy-3-methylglutaryl-coenzyme A reductase (HMGCR) playing key roles. HMGCS1 is a cytoplasmic enzyme upstream of HMGCR in the mevalonate pathway and can condense acetyl-CoA and acetoacetyl-CoA into HMG-CoA [36], a key enzyme in the biosynthesis of liver cholesterol. HMGCR is a rate-limiting enzyme in cholesterol synthesis, and increased HMGCR activity increases cholesterol synthesis in the liver. It has been found that inhibitors of HMGCS1 and HMGCR reduce liver cholesterol synthesis, thereby protecting against liver injury [37–39]. HMGCR appears to have a functional relationship with HIF-1α, as altering the expression of HIF-1α influences HMGCR expression in zebrafish [34], and HIF-1α can mediate the transcription of insulin-inducible gene 2 (Insig-2) leading to HMGCR degradation in the liver [40]. Another key enzyme in the mevalonate pathway, farnesyl diphosphate synthase (FDPS), is involved in the conversion of acetyl-CoA to cholesterol [41]; FDPS inhibitors, such as the bisphosphonate alendronate, reduce cholesterol synthesis and are used in the treatment of hypercholesterolemia [42, 43]. Polygala tenuifolia (PTE) down-regulates genes involved in lipid and cholesterol biosynthesis, including FDPS, to reduce lipid accumulation in an obese mouse model [44]. Our experimental results showed that Andro may inhibit the synthesis of cholesterol by down-regulating the expression of HMGCS1, HMGCR, and FDPS, thus inhibiting the inflammatory reaction and having a protective effect on liver injury. HMGCS1, HMGCR, and FDPS may thus be drug targets for the Andro inhibition of liver injury.

The MAPKs are a group of related serine-threonine protein kinases, and the MAPK cascade plays a key role in a wide variety of cellular activities, including proliferation, differentiation, apoptosis, oxidative stress, and inflammatory responses [45, 46]. Numerous studies have demonstrated a link between MAPK signaling and inflammation in many diseases [47], and the activation of the ERK1/2, JNK, and p38 pathways can increase the levels of pro-inflammatory factors, such as TNF-α, IL-1β, IL-6, and IL-8 [48, 49]. MAPK signaling is activated in LPS-induced liver injury [50–52]; thus, MAPK inhibition is closely involved in preventing and treating liver injury. While research has shown that Andro can inhibit inflammation through the MAPK pathway, most studies have focused on the roles of JNK, ERK1/2, and p38 in classic MAPK signaling [53, 54]. Here, the proteomic results indicated that Andro negatively regulates the MAPK cascade and down-regulates the expression of PBK and CAV1. PDZ-binding kinase (PBK, also known as TOPK) is a serine-threonine kinase belonging to the MAPK-kinase (MAPKK) family, that promotes phosphorylation of p38 MAPK [55], leading to the identification of p38 MAPK as a specific substrate of PBK [56] and suggesting the cell-type-dependent involvement of PBK in ERK/MAPK, p38 MAPK, and JNK signaling [57]. PBK can regulate cell survival, proliferation, growth, apoptosis, and inflammation [58, 59]. It has been observed that LPS increases PBK levels in leukemia cells while up-regulating the expression of inducible nitric oxide synthase (iNOS), suggesting that PBK may be involved in the inflammatory response or in inflammation-related diseases [60]. Paeonol-based derivatives can inhibit skin inflammation by inhibiting PBK-p38/JNK signaling pathway and down-regulating nitric oxide content in LPS-induced RAW264.7 cells [61]. Caveolin 1 (Cav1) is a structural protein of cell membranes and plays a role in regulating cholesterol distribution, inflammatory signal transduction, and other biological processes [62, 63]. Cav1 is involved in hepatocellular carcinoma and hepatocellular differentiation through its activation of MAPK signaling [64, 65], and inhibition of Cav1 is associated with the anti-inflammatory effects of some drugs [66–68]. Our experimental results showed that Andro may negatively regulate the MAPK cascade by down-regulating the expression of PBK and CAV1, thereby inhibiting MAPK signaling. These findings provide a new idea for Andro reduces inflammation through the MAPK pathway.

There is normally a balance between the production of ROS and reactive nitrogen species (RNS) and oxidant scavenging in the body, and low ROS/RNS levels are essential for cell signaling and the maintenance of cell homeostasis [69]. Oxidative stress results from an altered balance between ROS and/or RNS production and the antioxidant defense capabilities [70]. The production of ROS is an important factor in liver injury [71, 72], and ROS can affect cellular structures such as hepatocyte proteins, lipids, and DNA, leading to liver injury [73]. LPS-induced liver injury is often accompanied by oxidative stress [52, 71], and inhibition of oxidative stress and inflammation can alleviate LPS-induced liver injury [74]. Antioxidants are, therefore, considered to be promising treatments for liver injury [75]. The peroxiredoxins (PRDXs) are a ubiquitous family of antioxidant enzymes, with six different PRDXs (PRDX1-PRDX6) currently known [76]. PRDXs can catalyze the breakdown of H_2O_2 and alkyl peroxides to eliminate intracellularly generated ROS, thereby protecting cells against oxidative stress [77]. Andro is a natural antioxidant that scavenges ROS, inhibits free radical-producing enzymes, and protects the mitochondria, thereby treating diseases caused by oxidative stress [14]. We found that Andro up-regulated PRDX1, PRDX4, and PRDX6 and that they formed major components in the PPI networks. It has been found that PRDX1 reduces ROS levels and inhibits apoptosis induced by NF-κB or MAPK signaling [78, 79], and PRDX1 can interact with pro-Caspase-1 (CASP1)

to block the assembly of the NLRP3 (NOD-, LRR-, and pyrin-domain containing protein 3) inflammasome complex, thus acting as a negative regulator of NLRP3 inflammasome activation [80]. PRDX4 is a secreted enzyme responsible for ROS scavenging both intracellularly and extracellularly and has a protective effect in cholestatic liver injury [81]. PRDX6 is a widely expressed antioxidant non-selenium glutathione peroxidase implicated in a variety of cellular activities [82]. PRDX6 protects against neuronal death caused by oxidative stress [83], and can reduce LPS-induced renal ROS concentrations and inactivate the p38 MAPK and JNK pathways, thereby attenuating LPS-induced acute kidney injury [84]. Therefore, Andro may inhibit oxidative stress by up-regulating the expression of PRDX1, PRDX4, and PRDX6, protecting against LPS-induced liver damage.

Conclusion

Andro protects against LPS-induced liver injury. Proteomic analysis showed that this effect was mediated by the inhibition of steroid metabolism, negative regulation of MAPK signaling, and reducing oxidative stress. HMGCS1, HMGCR, FDPS, PBK, CAV1, PRDX1, PRDX4, and PRDX6 may be the targets of Andro.

Methods

Drugs and reagents

Andro (98% purity) was obtained from Xi'an XiaoCao Plant Technology Co., Ltd. (Xi'an, China), LMH cells were obtained from the ATCC (No. CRL-2117), while LPS (Escherichia coli, serotype 055: B5) and Dimethyl Sulphoxide (DMSO) were from Sigma (St. Louis, MO, USA), Cell Counting Kit-8 (CCK-8) was from Dojindo Laboratories (Kamimashiki-gun, Kumamoto, Japan), and RPMI-1640 and fetal bovine serum (FBS) were from Gibco (Waltham, MA, USA).

Cell culture and cell proliferation-toxicity assays

LMH cells were cultured in RPMI-1640 with 10% FBS and 1% PS (penicillin-streptomycin) at 37 ℃, 5% CO_2, and saturated humidity. The cells were harvested for subsequent experiments when they had reached a density of at least $1\times10^4/cm^2$.

The cytotoxicity of Andro to LMH cells was quantified with CCK-8 assays. LMH cells (1×10^5/mL) were inoculated into 96-well plates (NEST, Hong Kong, China) and grown for 24 h at 37 ℃. Next, fresh RPMI-1640 medium containing different concentrations of Andro (0, 1, 5, 10, 20, 50, 100, 200, 400 μM) and 0.1% DMSO was added to each well, with three replicates used for each concentration. After incubation for 0, 12, 24, 48, 72, and 96 h, 10 μl CCK-8 solution was added to each well and allowed to incubate for 2 h at 37 ℃, after which the optical densities (OD values) at 450 nm were read in a microplate reader (Varioskan LUX, Thermo, USA).

Effects of Andro on ALT and AST in LMH cells

NC group was treated with 0.1% DMSO and the LPS group was treated with 0.1% DMSO and 10 μg/ml LPS for 24 h [85]. Cells in the LPS-Andro group were pretreated with 1, 2, and 5 μM Andro and 0.1% DMSO for 1 h, followed by treatment with 10 μg/ml LPS for 24 h, with three replicates in each group. Lastly, ALT and AST activities in the culture supernatants were measured using an automatic biochemical analyzer (Chemray 240, Shenzhen Rayto Life and Analytical Sciences Co., Ltd. China).

Sample preparation

The proteomic analysis included three groups, namely, the NC, LPS, and LPS-Andro groups. Cells were lysed with 8 M Urea/100 mM Tris-Cl and ultrasonication. Dithiothreitol (DTT, 10 mM) was added and incubated at 37 ℃ for 1 h, followed by alkylation with 40 mM iodoacetamide (30 min, room temperature in the dark). Protein concentrations were determined using the Bradford method. The urea solution was reduced to below 2 M by dilution with 100 mM Tris-HCl, and the proteins were digested at a 1:50 trypsin:protein (w/w) ratio overnight at 37 °C. Digestion was halted with TFA and the samples were centrifuged (12,000×g, 15 min). The supernatants were retained and desalinated using SEP-PAK C18, after which the material was drained and stored at -20 °C.

Isobaric TMT was used for DEP identification. TMT labeling was conducted in accordance with the provided directions. Specifically, after reconstitution of the peptides in TMT buffer, the individual samples were labeled using different TMT labels. After mixing, the samples were desalted on SEP-PAK C18 and fractionated into 15 fractions by high-pH reverse-phase chromatography. The individual fractions were vacuum-dried and stored at -80 °C.

LC-MS/MS analysis

LC-MS/MS was performed using an Orbitrap Exploris 480 mass spectrometer coupled with an Easy-nLC 1200 system. After loading through the auto-sampler, the peptides were separated on a C18 analytical column (75 μm × 25 cm, C18, 1.9 μm, 100Å). The gradient was set up with mobile phase A (0.1% formic acid) and mobile phase B (80% ACN, 0.1% formic acid) and a flow rate of 300 nL/min. The DDA mode consisted of one full-scan mass spectrum (R=60 K, AGC=300%, max IT=20 ms, scan range=350–1500 *m/z*) followed by 20 MS/MS events (R=15 K, AGC=100%, max IT=auto, cycle time=2 s, TurboTMT enabled). The HCD collision energy was set

to 35, with a 1.2 Da isolation window and 35-s target ion exclusion.

Database search

The raw MS data were analyzed with MaxQuant v1.6.6 using the Andromeda database search algorithm. The spectra files were searched against the UniProt.Proteome. Chicken.20,201,018.fasta database using the following parameters: TMT mode was checked for quantification; Variable modifications, Oxidation (M), Acetyl (Protein N-term) & Deamidation (NQ) ; Fixed modifications, Carbamidomethyl (C); Digestion, Trypsin/P; The MS1 match tolerance was set as 20 ppm for the first search and 4.5 ppm for the main search; the MS2 tolerance was set as 20 ppm. The results were filtered using an FDR of 1% for both proteins and peptides. After removal of decoy hits, contaminants, or proteins only identified by sites, the identified proteins were used for further analysis.

Bioinformatics analysis

The identified DEPs were submitted to GO (http://geneontology.org/) and KEGG (http://www.genome.jp/kegg/) for annotation and pathway analysis respectively [86–88], using a threshold of $P<0.05$ to indicate significant enrichment. Subcellular localization and upregulation and downregulation numbers were predicted using PSORTb and WoLF PSORT. Protein-protein interaction (PPI) networks were constructed by STRING (http://string-db.org/), and used k-means method to further cluster analysis (the number clusters: 3).

Statistical analysis

GraphPad Prism (Version 9.0, San Diego, USA) was used for analysis and the compilation of graphs. Differences between two groups were determined by t-tests, the difference between LPS group and NC group was represented by #, and # $P<0.001$, the difference between LPS-Andro group and LPS group was represented by *, and * $P<0.05$, ** $P<0.01$, and *** $P<0.001$.

Supplementary Information

The online version contains supplementary material available at https://doi.org/10.1186/s12917-023-03758-2.

Supplementary Material 1

Supplementary Material 2

Acknowledgements

Not applicable.

Author contributions

PQH designed the experiment and revised the manuscript. GSH completed the experiment and drafted the manuscript. LWQ, LHM and BYJ participated in improving the experiment. WLZ, WDL and ZFW participated in collecting and preparing the samples. All authors contributed to the article and approved the submitted version.

Funding

This work was supported by Academic Restoration Scientific Research Project of Shanxi Agricultural University (2020xshf16) and National Natural Science Foundation of China (32273089).

Data Availability

The mass spectrometry proteomics data have been deposited to the ProteomeXchange Consortium (http://proteomecentral.proteomexchange.org) via the iProX partner repository with the dataset identifier PXD037079.

Declarations

Competing interest

The authors declare no competing financial interest.

Ethics approval and consent to participate

Not applicable.

Consent for publication

Not applicable.

Received: 8 March 2023 / Accepted: 27 September 2023
Published online: 10 October 2023

References

1. Liu A, Wang W, Fang H, Yang Y, Jiang X, Liu S, Hu J, Hu Q, Dahmen U, Dirsch O. Baicalein protects against polymicrobial sepsis-induced liver injury via inhibition of inflammation and apoptosis in mice. Eur J Pharmacol. 2015;748:45–53.
2. Sarba EJ, Kelbesa KA, Bayu MD, Gebremedhin EZ, Borena BM, Teshale A. Identification and antimicrobial susceptibility profile of Escherichia coli isolated from backyard chicken in and around ambo, Central Ethiopia. BMC Vet Res. 2019;15(1):85.
3. Tang Q, Li W, Dai N, Gao Y, Han Y, Cheng G, Gu C. The role of necroptosis, apoptosis, and inflammation in Fowl Cholera-Associated Liver Injury in a chicken model. Avian Dis. 2017;61(4):491–502.
4. Xie S, Li Y, Zhao S, Lv Y, Yu Q. Salmonella infection induced intestinal crypt hyperplasia through Wnt/beta-catenin pathway in chicken. Res Vet Sci. 2020;130:179–83.
5. Morrison DC, Ryan JL. Endotoxins and disease mechanisms. Annu Rev Med. 1987;38:417–32.
6. Tan Y, Kagan JC. A cross-disciplinary perspective on the innate immune responses to bacterial lipopolysaccharide. Mol Cell. 2014;54(2):212–23.
7. Wang Z, Ka SO, Han YT, Bae EJ. Dihydropyranoaurone compound damaurone D inhibits LPS-induced inflammation and liver injury by inhibiting NF-kappaB and MAPK signaling independent of AMPK. Arch Pharm Res. 2018;41(3):314–23.
8. Jayakumar T, Hou SM, Chang CC, Fong TH, Hsia CW, Chen YJ, Huang WC, Saravanabhavan P, Manubolu M, Sheu JR et al. Columbianadin Dampens in Vitro inflammatory actions and inhibits Liver Injury via Inhibition of NF-kappaB/MAPKs: impacts on ()OH radicals and HO-1 expression. Antioxid (Basel) 2021, 10(4).
9. Lv H, Yang H, Wang Z, Feng H, Deng X, Cheng G, Ci X. Nrf2 signaling and autophagy are complementary in protecting lipopolysaccharide/d-galactosamine-induced acute liver injury by licochalcone A. Cell Death Dis. 2019;10(4):313.
10. Jaeschke H. Reactive oxygen and mechanisms of inflammatory liver injury. J Gastroenterol Hepatol. 2000;15(7):718–24.
11. Shen K, Xi Z, Xie J, Wang H, Xie C, Lee CS, Fahey P, Dong Q, Xu H. Guttiferone K suppresses cell motility and metastasis of hepatocellular carcinoma by restoring aberrantly reduced profilin 1. Oncotarget. 2016;7(35):56650–63.
12. Mei J, Yang R, Yang Q, Wan W, Wei X. Proteomic screening identifies the direct targets of chrysin anti-lipid depot in adipocytes. J Ethnopharmacol. 2021;267:113361.
13. Yang L, Zhang JH, Zhang XL, Lao GJ, Su GM, Wang L, Li YL, Ye WC, He J. Tandem mass tag-based quantitative proteomic analysis of lycorine treatment in highly pathogenic avian influenza H5N1 virus infection. PeerJ. 2019;7:e7697.

14. Mussard E, Cesaro A, Lespessailles E, Legrain B, Berteina-Raboin S, Toumi H. Andrographolide, a natural antioxidant: an update. Antioxid (Basel) 2019, 8(12).
15. Chua LS. Review on liver inflammation and antiinflammatory activity of Andrographis paniculata for hepatoprotection. Phytother Res. 2014;28(11):1589–98.
16. Pan CW, Yang SX, Pan ZZ, Zheng B, Wang JZ, Lu GR, Xue ZX, Xu CL. Andrographolide ameliorates d-galactosamine/lipopolysaccharide-induced acute liver injury by activating Nrf2 signaling pathway. Oncotarget. 2017;8(25):41202–10.
17. Wang L, Cao F, Zhu LL, Liu P, Shang YR, Liu WH, Dong X, Bao HD, Gong P, Wang ZY. Andrographolide impairs alpha-naphthylisothiocyanate-induced cholestatic liver injury in vivo. J Nat Med. 2019;73(2):388–96.
18. De Castro C, Holst O, Lanzetta R, Parrilli M, Molinaro A. Bacterial lipopolysaccharides in plant and mammalian innate immunity. Protein Pept Lett. 2012;19(10):1040–4.
19. Lai JL, Liu YH, Liu C, Qi MP, Liu RN, Zhu XF, Zhou QG, Chen YY, Guo AZ, Hu CM. Indirubin inhibits LPS-Induced inflammation via TLR4 abrogation mediated by the NF-kB and MAPK signaling pathways. Inflammation. 2017;40(1):1–12.
20. Guha M, Mackman N. LPS induction of gene expression in human monocytes. Cell Signal. 2001;13(2):85–94.
21. Yang Y, Zhao J, Song X, Li L, Li F, Shang J, Wang WW. Amygdalin reduces lipopolysaccharide-induced chronic liver injury in rats by down-regulating PI3K/AKT, JAK2/STAT3 and NF-kappaB signalling pathways. Artif Cells Nanomed Biotechnol. 2019;47(1):2688–97.
22. Yang XD, Sun SC. Targeting signaling factors for degradation, an emerging mechanism for TRAF functions. Immunol Rev. 2015;266(1):56–71.
23. Lalani AI, Zhu S, Gokhale S, Jin J, Xie P. TRAF molecules in inflammation and inflammatory diseases. Curr Pharmacol Rep. 2018;4(1):64–90.
24. Hacker H, Tseng PH, Karin M. Expanding TRAF function: TRAF3 as a tri-faced immune regulator. Nat Rev Immunol. 2011;11(7):457–68.
25. Gupta AS, Waters MR, Biswas DD, Brown LN, Surace MJ, Floros C, Siebenlist U, Kordula T. RelB controls adaptive responses of astrocytes during sterile inflammation. Glia. 2019;67(8):1449–61.
26. Yao H, Sun Y, Song S, Qi Y, Tao X, Xu L, Yin L, Han X, Xu Y, Li H, et al. Protective Effects of Dioscin against Lipopolysaccharide-Induced Acute Lung Injury through Inhibition of oxidative stress and inflammation. Front Pharmacol. 2017;8:120.
27. Zhou JX, Wink M. Evidence for anti-inflammatory activity of Isoliquiritigenin, 18beta Glycyrrhetinic Acid, Ursolic Acid, and the traditional chinese medicine plants Glycyrrhiza glabra and Eriobotrya japonica, at the Molecular Level. Med (Basel) 2019, 6(2).
28. Corcoran SE, O'Neill LA. HIF1alpha and metabolic reprogramming in inflammation. J Clin Invest. 2016;126(10):3699–707.
29. Semenza GL. Hypoxia-inducible factors in physiology and medicine. Cell. 2012;148(3):399–408.
30. Rius J, Guma M, Schachtrup C, Akassoglou K, Zinkernagel AS, Nizet V, Johnson RS, Haddad GG, Karin M. NF-kappaB links innate immunity to the hypoxic response through transcriptional regulation of HIF-1alpha. Nature. 2008;453(7196):807–11.
31. Cardoso D, Perucha E. Cholesterol metabolism: a new molecular switch to control inflammation. Clin Sci (Lond). 2021;135(11):1389–408.
32. Tall AR, Yvan-Charvet L. Cholesterol, inflammation and innate immunity. Nat Rev Immunol. 2015;15(2):104–16.
33. Anavi S, Hahn-Obercyger M, Madar Z, Tirosh O. Mechanism for HIF-1 activation by cholesterol under normoxia: a redox signaling pathway for liver damage. Free Radic Biol Med. 2014;71:61–9.
34. Tan T, Yu RMK, Wu RSS, Kong RYC. Overexpression and knockdown of Hypoxia-Inducible factor 1 disrupt the expression of steroidogenic enzyme genes and early embryonic development in zebrafish. Gene Regul Syst Bio. 2017;11:1177625017713193.
35. Ouyang S, Yao YH, Zhang ZM, Liu JS, Xiang H. Curcumin inhibits hypoxia inducible factor-1alpha-induced inflammation and apoptosis in macrophages through an ERK dependent pathway. Eur Rev Med Pharmacol Sci. 2019;23(4):1816–25.
36. Goldstein JL, Brown MS. Regulation of the mevalonate pathway. Nature. 1990;343(6257):425–30.
37. Ma X, Bai Y, Liu K, Han Y, Zhang J, Liu Y, Hou X, Hao E, Hou Y, Bai G. Ursolic acid inhibits the cholesterol biosynthesis and alleviates high fat diet-induced hypercholesterolemia via irreversible inhibition of HMGCS1 in vivo. Phytomedicine. 2022;103:154233.
38. Dai W, Wang K, Zhen X, Huang Z, Liu L. Magnesium isoglycyrrhizinate attenuates acute alcohol-induced hepatic steatosis in a zebrafish model by regulating lipid metabolism and ER stress. Nutr Metab (Lond). 2022;19(1):23.
39. Wu YR, Li L, Sun XC, Wang J, Ma CY, Zhang Y, Qu HL, Xu RX, Li JJ. Diallyl disulfide improves lipid metabolism by inhibiting PCSK9 expression and increasing LDL uptake via PI3K/Akt-SREBP2 pathway in HepG2 cells. Nutr Metab Cardiovasc Dis. 2021;31(1):322–32.
40. Hwang S, Nguyen AD, Jo Y, Engelking LJ, Brugarolas J, DeBose-Boyd RA. Hypoxia-inducible factor 1alpha activates insulin-induced gene 2 (Insig-2) transcription for degradation of 3-hydroxy-3-methylglutaryl (HMG)-CoA reductase in the liver. J Biol Chem. 2017;292(22):9382–93.
41. Li K, Li H, Zhang K, Zhang J, Hu P, Li Y, Gu H, Liu HY, Yang Z, Cai D. Orphan Nuclear Receptor RORgamma Modulates the Genome-Wide Binding of the Cholesterol Metabolic Genes during Mycotoxin-Induced Liver Injury. *Nutrients* 2021, 13(8).
42. Griffin S, Preta G, Sheldon IM. Inhibiting mevalonate pathway enzymes increases stromal cell resilience to a cholesterol-dependent cytolysin. Sci Rep. 2017;7(1):17050.
43. Wasko BM, Smits JP, Shull LW, Wiemer DF, Hohl RJ. A novel bisphosphonate inhibitor of squalene synthase combined with a statin or a nitrogenous bisphosphonate in vitro. J Lipid Res. 2011;52(11):1957–64.
44. Wang CC, Yen JH, Cheng YC, Lin CY, Hsieh CT, Gau RJ, Chiou SJ, Chang HY. Polygala tenuifolia extract inhibits lipid accumulation in 3T3-L1 adipocytes and high-fat diet-induced obese mouse model and affects hepatic transcriptome and gut microbiota profiles. Food Nutr Res. 2017;61(1):1379861.
45. Guo YJ, Pan WW, Liu SB, Shen ZF, Xu Y, Hu LL. ERK/MAPK signalling pathway and tumorigenesis. Exp Ther Med. 2020;19(3):1997–2007.
46. Haston S, Pozzi S, Carreno G, Manshaei S, Panousopoulos L, Gonzalez-Meljem JM, Apps JR, Virasami A, Thavaraj S, Gutteridge A, et al. MAPK pathway control of stem cell proliferation and differentiation in the embryonic pituitary provides insights into the pathogenesis of papillary craniopharyngioma. Development. 2017;144(12):2141–52.
47. Hilliard A, Mendonca P, Soliman KFA. Involvement of NFkB and MAPK signaling pathways in the preventive effects of Ganoderma lucidum on the inflammation of BV-2 microglial cells induced by LPS. J Neuroimmunol. 2020;345:577269.
48. Dong N, Li X, Xue C, Zhang L, Wang C, Xu X, Shan A. Astragalus polysaccharides alleviates LPS-induced inflammation via the NF-kappaB/MAPK signaling pathway. J Cell Physiol. 2020;235(7–8):5525–40.
49. Xie W, Wang M, Chen C, Zhang X, Melzig MF. Hepatoprotective effect of isoquercitrin against acetaminophen-induced liver injury. Life Sci. 2016;152:180–9.
50. Wang H, Wei X, Wei X, Sun X, Huang X, Liang Y, Xu W, Zhu X, Lin X, Lin J. 4-hydroxybenzo[d]oxazol-2(3H)-one ameliorates LPS/D-GalN-induced acute liver injury by inhibiting TLR4/NF-kappaB and MAPK signaling pathways in mice. Int Immunopharmacol. 2020;83:106445.
51. He G, Zhao Q, Zhao Y, Zong Y, Gu S, Li M, Li R, Sun J. Deer antler based active ingredients have protective effects on LPS/d-GalN-induced acute liver injury in mice through MAPK and NF-kappaB signalling pathways. Pharm Biol. 2022;60(1):1077–87.
52. Lim JY, Lee JH, Yun DH, Lee YM, Kim DK. Inhibitory effects of nodakenin on inflammation and cell death in lipopolysaccharide-induced liver injury mice. Phytomedicine. 2021;81:153411.
53. Li Y, He S, Tang J, Ding N, Chu X, Cheng L, Ding X, Liang T, Feng S, Rahman SU, et al. Andrographolide inhibits inflammatory cytokines secretion in LPS-Stimulated RAW264.7 cells through suppression of NF-kappaB/MAPK signaling pathway. Evid Based Complement Alternat Med. 2017;2017:8248142.
54. Yang R, Liu S, Zhou J, Bu S, Zhang J. Andrographolide attenuates microglia-mediated Abeta neurotoxicity partially through inhibiting NF-kappaB and JNK MAPK signaling pathway. Immunopharmacol Immunotoxicol. 2017;39(5):276–84.
55. Dougherty JD, Garcia AD, Nakano I, Livingstone M, Norris B, Polakiewicz R, Wexler EM, Sofroniew MV, Kornblum HI, Geschwind DH. PBK/TOPK, a proliferating neural progenitor-specific mitogen-activated protein kinase kinase. J Neurosci. 2005;25(46):10773–85.
56. Abe Y, Matsumoto S, Kito K, Ueda N. Cloning and expression of a novel MAPKK-like protein kinase, lymphokine-activated killer T-cell-originated protein kinase, specifically expressed in the testis and activated lymphoid cells. J Biol Chem. 2000;275(28):21525–31.
57. Huang H, Lee MH, Liu K, Dong Z, Ryoo Z, Kim MO. PBK/TOPK: an effective drug target with diverse therapeutic potential. Cancers (Basel) 2021, 13(9).

58. Zhao R, Choi BY, Wei L, Fredimoses M, Yin F, Fu X, Chen H, Liu K, Kundu JK, Dong Z, et al. Acetylshikonin suppressed growth of colorectal tumour tissue and cells by inhibiting the intracellular kinase, T-lymphokine-activated killer cell-originated protein kinase. Br J Pharmacol. 2020;177(10):2303–19.
59. Zhao R, Huang H, Choi BY, Liu X, Zhang M, Zhou S, Song M, Yin F, Chen H, Shim JH, et al. Cell growth inhibition by 3-deoxysappanchalcone is mediated by directly targeting the TOPK signaling pathway in colon cancer. Phytomedicine. 2019;61:152813.
60. Park JH, Jeong YJ, Won HK, Choi SY, Park JH, Oh SM. Activation of TOPK by lipopolysaccharide promotes induction of inducible nitric oxide synthase through NF-kappaB activity in leukemia cells. Cell Signal. 2014;26(5):849–56.
61. Wu J, Zhu R, Cao GM, Du JC, Liu X, Diao LZ, Zhang ZY, Hu YS, Liu XH, Shi JB. Discovery of novel paeonol-based derivatives against skin inflammation in vitro and in vivo. J Enzyme Inhib Med Chem. 2022;37(1):817–31.
62. Chidlow JH Jr., Sessa WC. Caveolae, caveolins, and cavins: complex control of cellular signalling and inflammation. Cardiovasc Res. 2010;86(2):219–25.
63. Qin L, Zhu N, Ao BX, Liu C, Shi YN, Du K, Chen JX, Zheng XL, Liao DF. Caveolae and Caveolin-1 integrate reverse cholesterol transport and inflammation in atherosclerosis. Int J Mol Sci. 2016;17(3):429.
64. Zhang C, Wu Q, Huang H, Chen X, Huang T, Li W, Liu Y, Zhang J. Caveolin-1 promotes rfng expression via Erk-Jnk-p38 signaling pathway in mouse hepatocarcinoma cells. J Physiol Biochem. 2019;75(4):549–59.
65. Guan X, Wang N, Cui F, Liu Y, Liu P, Zhao J, Han C, Li X, Leng Z, Li Y, et al. Caveolin-1 is essential in the differentiation of human adipose-derived stem cells into hepatocyte-like cells via an MAPK pathway-dependent mechanism. Mol Med Rep. 2016;13(2):1487–94.
66. Tsai TH, Tam K, Chen SF, Liou JY, Tsai YC, Lee YM, Huang TY, Shyue SK. Deletion of caveolin-1 attenuates LPS/GalN-induced acute liver injury in mice. J Cell Mol Med. 2018;22(11):5573–82.
67. Yuan H, Hou Q, Feng X, Zhang Y, Yang F, Ge R, Li Q. 5,2'-Dibromo-2,4',5'-trihydroxydiphenylmethanone Inhibits LPS-Induced Vascular Inflammation by Targeting the Cav1 Protein. Molecules 2022, 27(9).
68. Ren Y, Li L, Wang MM, Cao LP, Sun ZR, Yang ZZ, Zhang W, Zhang P, Nie SN. Pravastatin attenuates sepsis-induced acute lung injury through decreasing pulmonary microvascular permeability via inhibition of Cav-1/eNOS pathway. Int Immunopharmacol. 2021;100:108077.
69. Hamanaka RB, Chandel NS. Mitochondrial reactive oxygen species regulate cellular signaling and dictate biological outcomes. Trends Biochem Sci. 2010;35(9):505–13.
70. Paradies G, Paradies V, Ruggiero FM, Petrosillo G. Oxidative stress, cardiolipin and mitochondrial dysfunction in nonalcoholic fatty liver disease. World J Gastroenterol. 2014;20(39):14205–18.
71. Li Q, Tan Y, Chen S, Xiao X, Zhang M, Wu Q, Dong M. Irisin alleviates LPS-induced liver injury and inflammation through inhibition of NLRP3 inflammasome and NF-kappaB signaling. J Recept Signal Transduct Res. 2021;41(3):294–303.
72. Wang Y, Zhao Y, Wang Z, Sun R, Zou B, Li R, Liu D, Lin M, Zhou J, Ning S, et al. Peroxiredoxin 3 inhibits Acetaminophen-Induced Liver pyroptosis through the regulation of mitochondrial ROS. Front Immunol. 2021;12:652782.
73. Cichoz-Lach H, Michalak A. Oxidative stress as a crucial factor in liver diseases. World J Gastroenterol. 2014;20(25):8082–91.
74. Zhou H, Yang R, Wang W, Xu F, Xi Y, Brown RA, Zhang H, Shi L, Zhu D, Gong DW. Fc-apelin fusion protein attenuates lipopolysaccharide-induced liver injury in mice. Sci Rep. 2018;8(1):11428.
75. Jiang Z, Meng Y, Bo L, Wang C, Bian J, Deng X. Sophocarpine attenuates LPS-Induced Liver Injury and improves survival of mice through suppressing oxidative stress, inflammation, and apoptosis. Mediators Inflamm. 2018;2018:5871431.
76. Wood ZA, Schroder E, Robin Harris J, Poole LB. Structure, mechanism and regulation of peroxiredoxins. Trends Biochem Sci. 2003;28(1):32–40.
77. Rhee SG, Chae HZ, Kim K. Peroxiredoxins: a historical overview and speculative preview of novel mechanisms and emerging concepts in cell signaling. Free Radic Biol Med. 2005;38(12):1543–52.
78. Ding C, Fan X, Wu G. Peroxiredoxin 1 - an antioxidant enzyme in cancer. J Cell Mol Med. 2017;21(1):193–202.
79. Guo W, Liu X, Li J, Shen Y, Zhou Z, Wang M, Xie Y, Feng X, Wang L, Wu X. Prdx1 alleviates cardiomyocyte apoptosis through ROS-activated MAPK pathway during myocardial ischemia/reperfusion injury. Int J Biol Macromol. 2018;112:608–15.
80. Liu W, Guo W, Zhu Y, Peng S, Zheng W, Zhang C, Shao F, Zhu Y, Hang N, Kong L, et al. Targeting Peroxiredoxin 1 by a Curcumin Analogue, AI-44, inhibits NLRP3 inflammasome activation and attenuates Lipopolysaccharide-Induced Sepsis in mice. J Immunol. 2018;201(8):2403–13.
81. Zhang J, Guo X, Hamada T, Yokoyama S, Nakamura Y, Zheng J, Kurose N, Ishigaki Y, Uramoto H, Tanimoto A et al. Protective Effects of Peroxiredoxin 4 (PRDX4) on Cholestatic Liver Injury. Int J Mol Sci 2018, 19(9).
82. Chowhan RK, Rahaman H, Singh LR. Structural basis of peroxidase catalytic cycle of human Prdx6. Sci Rep. 2020;10(1):17416.
83. Singh SP, Chhunchha B, Fatma N, Kubo E, Singh SP, Singh DP. Delivery of a protein transduction domain-mediated Prdx6 protein ameliorates oxidative stress-induced injury in human and mouse neuronal cells. Am J Physiol Cell Physiol. 2016;310(1):C1–16.
84. Lee DH, Park JH, Han SB, Yoon DY, Jung YY, Hong JT. Peroxiredoxin 6 overexpression attenuates lipopolysaccharide-induced acute kidney injury. Oncotarget. 2017;8(31):51096–107.
85. Wang B, Cui Y, Zhang Q, Wang S, Xu S. Selenomethionine alleviates LPS-induced JNK/NLRP3 inflammasome-dependent necroptosis by modulating miR-15a and oxidative stress in chicken lungs. Metallomics 2021, 13(8).
86. Kanehisa M, Goto S. KEGG: kyoto encyclopedia of genes and genomes. Nucleic Acids Res. 2000;28(1):27–30.
87. Kanehisa M. Toward understanding the origin and evolution of cellular organisms. Protein Sci. 2019;28(11):1947–51.
88. Kanehisa M, Furumichi M, Sato Y, Kawashima M, Ishiguro-Watanabe M. KEGG for taxonomy-based analysis of pathways and genomes. Nucleic Acids Res. 2023;51(D1):D587–92.

Publisher's Note